

Received May 22, 2020, accepted June 6, 2020, date of publication June 10, 2020, date of current version June 26, 2020.

Digital Object Identifier 10.1109/ACCESS.2020.3001342

Outage Analysis for Millimeter-Wave Fronthaul Link of UAV-Aided Wireless Networks

GIANLUCA FONTANESI¹, (Graduate Student Member, IEEE),

ANDING ZHU¹, (Senior Member, IEEE), AND HAMED AHMADI^{1,2}, (Senior Member, IEEE)

¹School of Electrical and Electronic Engineering, University College Dublin, Dublin 4, D04 V1W8 Ireland

²Department of Electronic Engineering, University of York, York YO10 5DD, U.K.

Corresponding author: Hamed Ahmadi (hamed.ahmadi@york.ac.uk)

This work was supported in part by the Irish Research Council under Grant GOIPG/2017/1741, and in part by the Science Foundation Ireland under Grant 13/RC/2077 and Grant 17/NSFC/4850.

ABSTRACT Unmanned Aerial Vehicle (UAV)-wireless networks represent a promising solution to expand the reach of mobile connectivity beyond current boundaries. When Distributed Units (DUs) are deployed on the UAV, the high rate requirement on the wireless Fronthaul (FH) link between the UAV-DU and the terrestrial network poses a major challenge. To address the capacity demand of the FH network, we investigate the outage probability at millimeter Wave (mmWave) and sub-6 GHz frequency for different blockage environments and UAV heights. Utilizing a stochastic geometry framework, we first derive analytical approximate expressions for the outage probability of the FH link and we observe generally a good agreement with the simulation results for different UAV heights. In addition, numerical results for different urban densities show that the FH outage probability is minimized choosing an optimal UAV-DU altitude. We further analyze the impact of the antenna gain for two candidate mmWave frequencies on the FH link. High mmWave bands need sharp directional beamforming and large transmit bandwidth to outperform low mmWave bands in term of rate outage. Finally, our results show the impact on the outage probability of the FH overhead, that scales with the number of antenna elements, for different protocol splits.

INDEX TERMS Unmanned aerial vehicle, fronthaul, mmWave, sub-6 GHz, outage.


I. INTRODUCTION

Traditional Base Stations (BSs), due to their stationary location and low flexibility, are not optimized to satisfy the service requirements of applications such as search and rescue, disaster aid and reconnaissance. Unmanned Aerial Vehicle (UAV)-aided wireless networks, instead, have the flexibility and autonomy to serve these scenarios and open up a wide spectrum of opportunities [1]. In addition, the use of UAV-aided wireless networks at millimeter Wave (mmWave) frequency bands represents a use case that can go beyond the performance of the Fifth Generation (5G) networks [2].

A crucial design choice for the introduction of aerial BSs concerns the level of processing centralization in the network. Given the intrinsic limitations of UAV payload and battery capacity, it is desirable to keep the computational complexity and the energy consumption on the UAV as low as possible. This can be achieved by adopting a distributed configuration, where only the Radio Frequency (RF)

functions are performed at the UAV. In 5G New Radio (NR), the radio processing and baseband functions are generally referred as Distributed Unit (DU) and a Centralized Unit (CU) [3]. If only the DU is deployed on the body of the UAV, the payload becomes smaller and lighter, which can result in more efficient use of processing resources and reduced energy consumption. In this distributed system, the link connecting the aerial DU to the ground CU is conventionally referred as Fronthaul (FH). Ensuring a reliable FH link is of vital importance for the control and operations of the UAV communication. However, for an aerial distributed configuration the fronthaul rate requirement is high and poses the major challenge. This motivates us to investigate the outage probability of the FH. The reliability of the FH network between the CU and the UAV-DU is challenging also due to the low latency and limitation of available energy on the UAV. However, we leave the investigation of these aspects for a future work.

Given the fact that wired links are impractical, recent works have considered using optical technologies, e.g., Free Space Optics (FSO), especially if High Altitude Platform (HAP)

The associate editor coordinating the review of this manuscript and approving it for publication was Peng-Yong Kong .

and a long range link is considered [4]. However, FSO is very sensitive to inclement weather conditions and pointing error. If using wireless technologies, two main candidates have been proposed: sub-6 GHz and mmWave (Fig. 1). The sub-6 GHz link is less sensitive to obstacles and thus can be a good choice in dense-obstacle environments. The mmWave link offers larger available bandwidth as well as beamforming gain and higher data rates [5]. In addition, the performance of a mmWave link increases dramatically if no obstacles are present. UAV networks can take advantage of this as it is possible for them to modify the altitude of the UAV to obtain an unobstructed path.

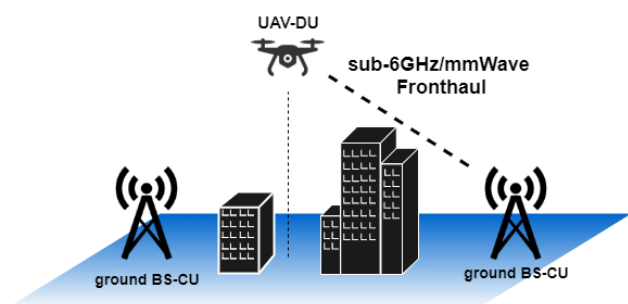


FIGURE 1. An illustration of the scenario under investigation.

Taking into consideration the above mentioned aspects and challenges, we are motivated to investigate the wireless technology that minimizes the outage probability of an FH link to a UAV-DU for different system parameters. The mathematical approach known as stochastic geometry, which models the locations of BSs as points of a Poisson Point Process (PPP), offers good estimates of the outage probability in a network without conducting expensive field tests.

Stochastic geometry has been extensively used for the tractable performance analysis of terrestrial communication systems [6], [7] and recently, it has also been intensively applied to UAV communications. A significant effort has been dedicated to the analytical study the scenario of a UAV or multiple UAVs serving User Equipments (UEs) on the ground. Mozaffari *et al.* [8] studied a UAV-aided network with underlaid Device-to-Device (D2D) links and derived the average coverage probability and throughput. The work in [9] derives the optimal altitude to maximize the coverage on the ground. In [10] the coverage probability for a typical user on the ground served by a network of UAV-BSs is derived considering Line of Sight (LoS) and Non-Line of Sight (NLoS) links, whereas the work in [11] assumes a terrestrial channel model to derive an exact analytical expression for the coverage probability of uniformly distributed low altitude UAV-BSs. A more practical scenario is presented in [12], where the authors investigate and derive the theoretical analysis of Downlink (DL) channel performance of both aerial and terrestrial users in an existing Long Term Evolution (LTE) network. The performance of a vertical Heterogeneous Network (HetNet) comprising aerial BSs and terrestrial BSs is investigated in [13]. Similarly, [14] analyzes the

performance of an aerial UE served by terrestrial and aerial BSs.

The aforementioned research contributions give an indication on the performance of aerial BSs in UAV-aided wireless networks when deployed alone or with terrestrial BSs. However, all these works are focused on sub-6 GHz scenarios. The sub-6 GHz framework available in literature is not directly suitable to the mmWave case since the mmWave scenario needs to reconsider and adapt the antenna pattern and fading channel model. The antenna pattern should be modeled to depict the sharp directional beam that enhances the desired signal and balances the severe path loss occurring at those frequencies. In addition, the fading model should consider the huge difference in path loss between the LoS and NLoS cases [15]. The work in [16] considers the problem of investigating a backhaul link to an aerial BS at sub-6 GHz and mmWave bands. The authors derive an exact backhaul coverage probability expression for different UAV heights. A general mmWave spatial framework to compute the average performance of a UAV aided network composed of an uplink and downlink phase, where the UAV acts as relay, is proposed in [17]. The authors derive the total system coverage probability and compare different mmWave carrier frequencies.

The above mentioned studies show that the access link between the UAV and the UEs has a good amount of valid published results. On the contrary, the investigation of a FH link to a UAV-DU as for Fig. 1 is at early stage. In more details, a question remains unsolved: can mmWave technology provide a FH link that is always available for different blockage environments and UAV heights? The 5G NR is believed to adopt the mmWave in addition to a back-up sub-6 GHz band but, for the scenario of mmWave UAV-aided networks, we believe there is a lack of work that investigates potential outage states of the FH link. Thus, the goal of this paper is to answer the above question.

The contributions of this paper can be listed broadly as follows:

1) TRACTABLE MODEL

A tractable and general model is introduced to derive the outage probability for a FH link between terrestrial BSs, distributed as PPP on the ground, to a UAV-DU at different heights. An approximated function of the ground-to-air LoS probability is applied. In contrast with other works, we utilize the upper bound on the incomplete Gamma function to derive the approximated expressions that are able to characterize both a sub-6 GHz and a mmWave FH links. We identify two cases that approximate the general coverage expressions in order to simplify the analysis and enhance the evaluation efficiency.

2) VALIDATION AND ANALYSIS

We validate the derived expression with Monte Carlo (MC) simulations, at both mmWave and sub-6 GHz. Moreover, we show that in terms of mmWave communication, NLoS

transmissions can be ignored when the UAV height increases and the density of blockage environments decreases.

3) PERFORMANCE AND INSIGHT

We show that there exists an optimal altitude that minimizes the FH outage probability for different blockage environments and ground BS densities. Moreover, considering a target rate, the rate outage probability of the FH link is lower at sub-6 GHz for low UAV heights. At higher altitude instead, the mmWave link has a higher probability to satisfy the target rate of the FH. We further analyze the impact of the antenna gain for two candidate mmWave frequencies on the FH link. Furthermore, we discuss different split protocol options between the CU and the UAV-DU and give an insight of the effect of a low protocol split when hundreds of antennae are deployed at the BS to mitigate the path loss of high mmWave bands.

The rest of the paper is organized as follows: Section II introduces the network model, including the ground-to-air channel model and the blockage model. Section III describes the derivation of the outage probability for the proposed network model. Section IV provides the validation of the derived equations and numerical results. Section V concludes the paper.

II. SYSTEM MODEL

We consider a terrestrial network in which CUs are in the ground BSs, providing a ground-to-air FH link to an arbitrary number of DUs mounted on UAVs. The ground BSs are randomly distributed with density λ [BS/m^2] and all transmitting at the same transmission power P_{TX} at height h_{BS} . Without loss of generality, we focus our outage analysis on one typical UAV-DU hovering at position X_0 (origin), at a certain height h_{UAV} , where $h_{UAV} > h_{BS}$. Hence, we set $h_{diff} = h_{UAV} - h_{BS}$. A summary of the notations that we use in the rest of the paper is provided in Table 1. The distance between a ground BS and the projection of the typical UAV-DU on the ground is denoted by z , while the link distance is denoted by d . Each BS and the UAV-DU can operate at sub-6 GHz and mmWave bands but we assume that data transmission occurs in a single frequency band at a time. In this work, we do not consider the access link between the UAV-DU and UEs on the ground. Next, we first characterize the ground-to-air channel and blockage, and then fading and beamforming model.

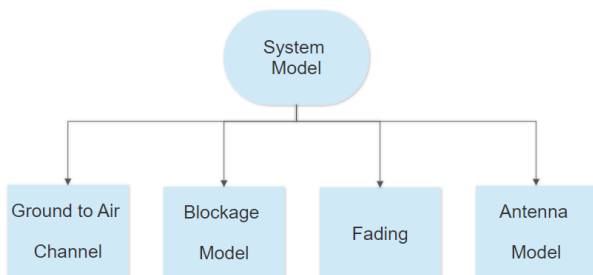


FIGURE 2. Overview of the sections described in the system model.

TABLE 1. Notation and symbols summary.

Notation	Description
PPP	Poisson Point Process
λ	density of ground BSs
h_{UAV}, h_{diff}	UAV height, UAV-BS height difference
f	fading
G, p	antenna gain, gain probability
$\theta_{BS}, \theta_{UAV}$	Ground BS, UAV main lobe beamwidth
G_0	antenna gain main link
m	Nakagami parameter
$I; L_I()$	Interference, Laplace transform of interference
$P_{TX}; \sigma_n^2$	Transmit Power of terrestrial BS, thermal noise power
α_L, α_{NL}	Path loss exponents for LoS and NLoS
f_{RL}, f_{RNL}	Distribution of the distance between the reference UAV and the closest LoS/NLoS ground BS
P_{LoS}, P_{NLoS}	LoS/NLoS Probability
a, b and c	Scenario parameters for LoS Probab.
P_{AL}, P_{ANL}	LoS/NLoS Association Probability
$P_{F,cov}(\lambda, \Gamma)$	Conditional coverage probability
P_{out}	Outage Probability
Γ	SINR threshold for successful fronthaul communication

A. GROUND TO AIR CHANNEL

The ground-to-air channel model is characterized by blockage, that divides the links between the terrestrial BSs on the ground and the reference UAV-DU between LoS and NLoS. Thus, two different pathloss functions for the LoS and NLoS cases can be identified, leading to:

$$l(d) = \begin{cases} l^L(d) = X_L d^{-\alpha_L}; & LoS : P_{LoS}(z) \\ l^{NL}(d) = X_{NL} d^{-\alpha_{NL}}; & NLoS : 1 - P_{LoS}(z), \end{cases} \quad (1)$$

where α_L and α_{NL} are the LoS and NLoS path loss exponents and X_L and X_{NL} are the intercepts of the LoS and NLoS path formulas. $P_{LoS}(z)$ and $P_{NLoS}(z)$, where $P_{NLoS}(z) = 1 - P_{LoS}(z)$, capture the occurrence of LoS and NLoS transmissions for a certain height h and horizontal distance z . The values of α_L , α_{NL} , X_L and X_{NL} are the result of field tests and are sensitive to the tested distances and test setup (e.g. height). For the ground-to-air model in the sub-6 GHz band these values have been standardized by the 3rd Generation Partnership Project (3GPP) in [18] for different UAV heights. At mmWave band, since no standardized results exist, the values used in recent works on UAV communication differ [16], [17]. We list these values in Table 2.

TABLE 2. Pathloss parameters for the mmWave band.

Parameter	28 GHz	70 GHz
α_L	2 [17], 2 [19], 2.09 [20]	2.25 [17], 2 [16]
α_{NL}	3 [17], 4 [19], 3.75 [20]	3.76 [17], 3.5 [16]
X_L	-61.4dB [17], -61.4dB [19], $10^{3.08}$ [20]	-69.7dB [16], -68dB [17]
X_{NL}	-61.4dB [17], -61.4dB [19], $10^{0.27}$ [20]	-69.7dB [16], -68dB [17]

B. BLOCKAGE MODEL

The International Telecommunication Union (ITU) in its technical report [21] defines three statistical parameters that characterize any urban environment: the ratio of land area covered by buildings to total land area (β_1), the mean number of buildings per unit area (β_2), and the height of buildings modeled by a Rayleigh Probability Density Function (PDF) with a scale parameter κ . Different types of environment can be obtained changing the above parameters as for [22, Table 1]. Hence, the LoS probability between a transmitter, of height h_{TX} , and a receiver, of height h_{RX} can be written as:

$$P_{LoS}(z) = \prod_{n=0}^{\gamma} \left[1 - \exp\left(-\frac{[h_{TX} - \frac{(n+\frac{1}{2})(h_{TX}-h_{RX})}{\gamma+1}]^2}{2\kappa^2}\right) \right], \quad (2)$$

where z denotes the ground distance between the transmitter and the receiver and $\gamma = \lfloor \frac{z\sqrt{\beta_1\beta_2}}{1000} - 1 \rfloor$. In our system model, h_{TX} is the height of the terrestrial BS while h_{RX} the height of the UAV-DU. The blockage model in (2) can be used for a wide spectrum range and it is suitable for both sub-6 GHz and mmWave scenarios [9]. In addition, it is suitable for any transmitter/receiver heights [9], and hence for both ground-to-UAV and UAV-to-ground transmissions. We focus and investigate a ground-to-UAV FH link and thus, we intend it for ground-to-UAV transmissions. However, the LoS probability in (2) is not a continuous but a step function of z . Thus, to ease the calculation of the LoS probability, similar to [14] we adopt the expression:

$$P_{LoS}(z) = -a \exp\left(-b\left(\arctan\left(\frac{h_{TX} - h_{RX}}{z}\right)\right)\right) + c, \quad (3)$$

where varying the tuple a, b and c leads to different environment (e.g. Dense Urban, Urban etc, see [14, Table 1]). Note that the popular P_{LoS} formulation derived in [9] is generally adopted for UAV-to-ground links, where the UEs on the ground are standardized at heights of 1.5/2 m. However, in our paper we investigate a ground-to-air FH link, where the transmitting BSs have greater height than terrestrial UEs. Hence, for the ground-to-air FH link under investigation the approximation in [9] is not suitable.

Due to the blockage effect and the LoS/NLoS propagation discussed above, the set of ground BSs in the terrestrial network providing a FH link to the UAV-DU can be divided into two independent PPPs. One non-homogeneous PPP Φ_L represents the terrestrial LoS BSs and has a density $\lambda P_{LoS}(z)$. Similarly, the NLoS BSs are seen from the UAV-DU as a PPP Φ_{NL} with density $\lambda(1 - P_{LoS}(z))$. The in-homogeneity of the processes Φ_L and Φ_{NL} has two main reasons. First, it follows from the dependency of the LoS probability on the distance z . Second, we assume that the LoS probabilities between different ground BS-UAV links are independent. This last assumption neglects the correlation in the LoS probability experienced by close BSs when transmitting to the UAV. It has been shown in [23] that ignoring such correlation

does not affect the accuracy of the Signal-to-Interference-plus-Noise Ratio (SINR) evaluation.

C. FADING

For the LoS/NLoS ground-to-air channels seen from the UAV-DU we assume independent Nakagami- m fading, where the shape parameter m captures a wide range of fading scenarios (when $m = 1$ it is namely Rayleigh fading). To the LoS and NLoS links can be assigned different Nakagami fading parameters that lead to different sub-6 GHz and mmWave propagation characteristics. Then under the Nakagami fading assumption, the channel fading power gains, denoted by f , follow a Gamma distribution with PDF given by $f_f(g) = \frac{m^m g^{m-1}}{\Gamma(m)} \exp(-mg)$, where $\Gamma(m)$ is the Gamma function. For a normalized gamma random variable h with parameter m and a constant $\epsilon > 0$, the probability $P(h < \epsilon)$ can be upper bounded as [15]:

$$P(h < \epsilon) < [1 - \exp(-\eta\epsilon)]^m \quad (4)$$

where $\eta = m(m!)^{-\frac{1}{m}}$. For analytical tractability the Nakagami parameter m is commonly considered positive integer.

D. ANTENNA MODEL AND BEAMFORMING

We consider that beamforming is applied both to ground BSs and UAV-DU. The UAV-DU and its associated BS are assumed to directly predict the optimal beam and adjust their steering orientation to achieve the maximum directionality gain with machine learning techniques [24]. Fluctuations in the orientation of UAV, due to wind loading effects, mechanical and control system resolutions, antenna and DU payload, that lead to beam misalignment are here not considered. These effects are described in [25]. For tractability of analysis, we approximate the antenna pattern by a sectored antenna model [15]. According with this model the antenna has a main lobe, whose average gain M depends on the type of antenna deployed, and a side lobe, with gain m . θ represents the main lobe beamwidth. We assume Uniform Planar Square Array (UPA) at the transmitter and receiver. The main lobe gain G is then proportional with the number of antenna elements N deployed. Due to beam alignment, $G_0 = M_{BS}M_{UAV}$ is the total maximum gain experienced in the desired link. Similar to [16] and [15], we assume the neighbor BSs are pointing randomly their main lobe, causing interference. It follows that interfering link will have a gain given by G_i ($i \in \{1, 2, 3, 4\}$) with uniform probability p_i , as follows:

$$\begin{cases} G_1 = M_{BS}M_{UAV} & w.p. & p_1 = \frac{\theta_{BS}}{2\pi} \frac{\theta_{UAV}}{2\pi} \\ G_2 = m_{BS}M_{UAV} & w.p. & p_2 = (1 - \frac{\theta_{BS}}{2\pi}) \frac{\theta_{UAV}}{2\pi} \\ G_3 = M_{BS}m_{UAV} & w.p. & p_3 = \frac{\theta_{BS}}{2\pi} (1 - \frac{\theta_{UAV}}{2\pi}) \\ G_4 = m_{BS}m_{UAV} & w.p. & p_4 = (1 - \frac{\theta_{BS}}{2\pi}) (1 - \frac{\theta_{UAV}}{2\pi}) \end{cases} \quad (5)$$

The above described system model is tractable for both the sub-6 GHz and mmWave. We now turn our attention to analyze the analytical performance of the fronthaul link and consider the way mmWave differ from the conventional sub-6GHz.

III. SINR OUTAGE PROBABILITY

The outage probability of the FH link from the terrestrial BS to the typical UAV can be derived computing the coverage probability that the reference UAV's SINR is above a predesignated threshold, that we define Γ . The outage probability can be then derived as $P_{OUT} = 1 - P(\text{SINR} > \Gamma)$.

We assume the UAV-DU to associate not the closest terrestrial BS, but to the one which yields the highest average received power [26]. Due to the difference in the values assigned to the LoS/NLoS propagation parameter X and α , it may happen that a far LoS-BS offers a better SINR than a closer NLoS (Fig. 3). However, based on this association rule, the LoS or NLoS terrestrial BS that is providing the strongest average received power is also the closest BS in LoS or NLoS. We call this the tagged BS. Note that in practice the UAV may receive interference only from a subset of transmitting BSs, but we here consider the worst case scenario, where all the non-associated BSs transmit at the same power and generate LoS and NLoS interference. The extension for dynamic interference will be an interesting work for further investigation.

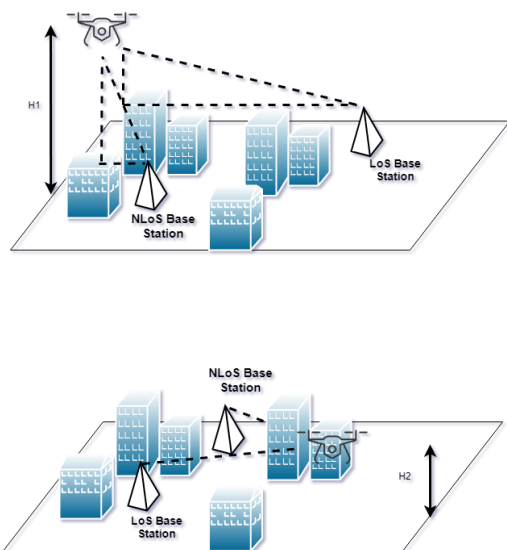


FIGURE 3. Association scenarios.

Thus, the general equation of the SINR at the UAV-DU is:

$$\text{SINR} = \frac{P_{TX}l(d)fG}{I + \sigma_n^2}, \quad (6)$$

where, P_{TX} denotes the terrestrial BS transmission power, f is Nakagami fading, G is the antenna gain, $l(d)$ the path loss and d the distance between the BS and the UAV-DU. I refers to

the aggregate interference power and σ_n^2 denotes the additive white Gaussian noise power.

Considering now that the UAV-DU associates with a LoS/NLoS BS x_i at distance R_ω , such that $R_\omega = \min_{\forall \omega \in \{L, NL\}, \forall x_i \in \Phi_\omega} d_\omega$, where $\omega \in \{L, NL\}$ denotes the LoS/NLoS link status of associated terrestrial BS, the SINR at the UAV-DU can be expressed as:

$$\text{SINR} = \frac{P_{TX}X_\omega R_\omega^{-\alpha_\omega} fG}{I + \sigma_n^2}. \quad (7)$$

Starting from the SINR expression in (7) we provide in the next sections a tractable approximation of the coverage probability that captures the dependency of several parameters for a mmWave link. As a benchmark, we will mention how to derive the corresponding sub-6 GHz expressions. Finally, we will derive the outage probability from the coverage probability.

A. APPROXIMATE COVERAGE PROBABILITY

The coverage probability can be written as a function of the random (Nakagami) fading effect as:

$$\begin{aligned} p_{F,cov}(\lambda, \Gamma) &= P_{F,cov}(\text{SINR} > \Gamma) \\ &= P_{F,cov}\left(\frac{P_{TX}X_\omega R_\omega^{-\alpha_\omega} fG}{I + \sigma_n^2} > \Gamma\right) \\ &= P_{F,cov}\left(f > \frac{\Gamma(I + \sigma_n^2)}{P_{TX}X_\omega R_\omega^{-\alpha_\omega} G}\right). \end{aligned} \quad (8)$$

The evaluation of the Cumulative Distribution Function (CDF) of the normalized gamma random variable f can be performed rigorously, solving higher order derivatives of the Laplace transform [27]. However, for large values of the fading shape parameter m , the computation complexity of the derivatives of the Laplace transform become cumbersome [11]. In [15] has been shown that the upper bound in (4) is a tight approximation to the CDF of a gamma variable. For this reason, in this paper, rather than the exact evaluation, we utilize for both the sub-6GHz and mmWave bands an upper bound based on (4).

In the next sections we first characterize the serving distance distribution, association probabilities and Laplace transform of interference. Then we derive the upper bound on the FH coverage probability. We will show that the approximation is tight in numerical simulations with different system parameters.

B. SERVING DISTANCE DISTRIBUTIONS AND ASSOCIATION PROBABILITIES

In this section, we provide the distribution of some relevant distances which will be used when we characterize the association probabilities and coverage probability. First, we provide the distribution of the distances between the typical UAV and the closest LoS/NLoS BS. The PDF of the distance between the UAV-DU and its closest LoS/NLoS BS,

$f_{R_L}(r)$ and $f_{R_{NL}}(r)$, can be obtained as:

$$f_{R_L}(r) = 2\pi\lambda r P_{LoS}(\sqrt{r^2 - h_{diff}^2}) \times \exp\left(-2\pi\lambda \int_{h_{diff}}^r P_{LoS}(\sqrt{t^2 - h_{diff}^2}) dt\right) \quad (9)$$

$$f_{R_{NL}}(r) = 2\pi\lambda r (1 - P_{LoS}(\sqrt{r^2 - h_{diff}^2})) \times \exp\left(-2\pi\lambda \int_{h_{diff}}^r (1 - P_{LoS}(\sqrt{t^2 - h_{diff}^2})) dt\right). \quad (10)$$

Proof: See Appendix A. \square

Secondly, we need to give a clear insight on the range over which the interfering ground-BSs are located. In the next lemma, we determine the range over which the interfering BSs are located, which will be useful when we present the main results of this paper.

Lemma 1: If the reference UAV-DU is associated with a LoS ground BS at distance r , the closest NLoS interferer can be at distance:

$$r_{I,NL} = \arg\{I^L(r) = I^{NL}(r_I)\}. \quad (11)$$

Proof: Considering the association rule presented above, the associated LoS ground BS is the closest in LoS and there are no other LoS ground BSs at distance smaller than r . With the assumption that $E[f] = E[G] = 1$, the NLoS ground BSs interferers will be at a distance no less than r_I that satisfies $X_L r^{-\alpha_L} = X_{NL} r_I^{-\alpha_{NL}}$. \square

Lemma 2: If the reference UAV-DU is associated with a NLoS ground BS at distance r , the closest LoS interferer can be at distance

$$r_{I,L} = \arg\{I^L(r_I) = I^{NL}(r)\} \quad (12)$$

Proof: Similar to Lemma 1 and therefore omitted. \square

C. ASSOCIATION PROBABILITY

Now we derive the probability that the reference UAV-DU connect to a BS in LoS or in NLoS.

Lemma 3: The probability that the UAV-DU is associated with a LoS terrestrial BS is given by:

$$P_{AL} = \int_{h_{diff}}^{\infty} \left(\exp\left(-2\pi\lambda \int_{h_{diff}}^{r_{I,NL}} t P_{NLoS}(\sqrt{t^2 - h_{diff}^2}) dt\right) \right) f_{R_L}(t) dt, \quad (13)$$

where P_{NLoS} is the NLoS probability and f_{R_L} is the probability density function (PDF) obtained in (9). The probability that the reference UAV-DU connect to a BS in NLoS is $P_{ANL} = 1 - P_{AL}$.

Proof: See Appendix B. \square

D. LAPLACE TRANSFORM OF INTERFERENCE

Given the interference distance and the association rule explained above, we can analyze here the interference seen at the reference UAV-DU. In the following section, we derive

the Laplace transform of interference power which will be a key intermediate result for the coverage probability. The general approach to the interference is the computation of the Laplace transform of a random variable I at s conditioned at the random distance R to the attached terrestrial BS [6]. Similarly to the case of an UE in a terrestrial network [15], the reference UAV-DU at the origin will see two independent components, due to the LoS and NLoS condition of the ground BSs. Thus, the total interference can be written as:

$$I = I_L + I_{NL} = \sum_{x_i \in \Phi_L/x_R} P_{TX} I^L(d) fG + \sum_{x_i \in \Phi_{NL}/x_R} P_{TX} I^{NL}(d) fG. \quad (14)$$

Using the independence and the probability generating functional (PGFL) of the PPPs with respect to the functions:

$$f_1(x) = E_{G,f} \left[\exp\left(-\sum_{x_i \in \Phi_L/x_R} s P_{TX} fG r^{-\alpha_L}\right) \right], \quad (15)$$

and

$$f_2(x) = E_{G,f} \left[\exp\left(-\sum_{x_i \in \Phi_{NL}/x_R} s P_{TX} fG r^{-\alpha_{NL}}\right) \right], \quad (16)$$

the Laplace transform of interference yields:

$$\begin{aligned} L_I(s) &= E[\exp(-sI)] \\ &= E[\exp(-sI_L)] \times E[\exp(-sI_{NL})] \\ &= E_{G,f} \left[\prod_{\omega \in \{L,NL\}} \exp\left(-2\pi \int_{d_\omega}^{\infty} (1 - \exp(-s P_{TX} I^\omega(t) fG)) \right. \right. \\ &\quad \left. \left. \times \lambda P_\omega(\sqrt{t^2 - h_{diff}^2}) dt\right) \right]. \end{aligned} \quad (17)$$

It is useful to note that (17) represents the main difference between the sub-6 GHz with the mmWave case. In fact, the $L_I(s)$ for the sub-6 GHz is directly obtained computing the moment generating function of the Gamma distribution [10], leading to:

$$\begin{aligned} L_I^{sub6}(s) &= \prod_{\omega \in \{L,NL\}} \exp\left(-2\pi\lambda \int_{d_\omega | P_{A\omega}}^{\infty} \left(1 - \left(\frac{m}{m + s P_{TX} I^\omega(t) G}\right)^m\right) \right. \\ &\quad \left. \times P_\omega(\sqrt{t^2 - h_{diff}^2}) dt\right), \end{aligned} \quad (18)$$

where $d_L | P_{AL} = r$, $d_{NL} | P_{AL} = r_{I,NL}$ and $d_L | P_{ANL} = r_{I,L}$, $d_{NL} | P_{ANL} = r$. Note that the Nakagami parameter m has different values for the sub-6 GHz for the LoS or NLoS case [10], [11]. The proof is here omitted since it is similar to [10].

For the mmWave instead, the randomness added in the interference from the Nakagami- m fading and the directivity gain from beamforming must be taken into consideration [5].

Thus, considering for the moment only the LoS case, (17) can be written as function of the gain G and f , as:

$$\begin{aligned} L_{I,L}^{mmWave}(s) &= \exp\left(-2\pi\lambda \int_r^\infty (1 - E_{G,f}[\exp(-sP_{TX}l^L(t)fG)]) \right. \\ &\quad \times P_{LoS}(\sqrt{t^2 - h_{diff}^2})tdt \Big) \\ &\stackrel{(a)}{=} \exp\left(-2\pi\lambda \int_r^\infty \left(1 - E_G\left[\left(1 + \frac{sP_{TX}GX_L}{mr^{\alpha_L}}\right)^{-m}\right]\right) \right. \\ &\quad \left. P_{LoS}(\sqrt{t^2 - h_{diff}^2})tdt \right) \end{aligned} \quad (19)$$

where (a) comes from the expectation of the normalized Gamma variable f . At this point, the derivation for a closed expression for the Laplace transform of the interference would impose to exploit the step property of equation (2) to substitute the above integral with a sum of weighted integrals [16], [17]. The derivation for this latter case is reported in Appendix C. Since the approximation in (3) is a continuous function, from (19) a simpler closed form of the Laplace transform can be written as:

$$\begin{aligned} L_{I,L}^{mmWave}(s) &= \exp\left(-2\pi\lambda P_{LoS}(\sqrt{r^2 - h_{diff}^2}) \right. \\ &\quad \left. E_G\left[\frac{r^2}{2}({}_2F_1(-\frac{2}{\alpha_L}, m; 1 - \frac{2}{\alpha_L}; -\frac{sP_{TX}G}{mX_L r^{\alpha_L/2}}) - 1)\right]\right) \\ &= \exp\left(-2\pi\lambda P_{LoS}(\sqrt{r^2 - h_{diff}^2}) \right. \\ &\quad \left. \sum_{i=1}^4 p_i \left[\frac{r^2}{2}({}_2F_1(-\frac{2}{\alpha_L}, m; 1 - \frac{2}{\alpha_L}; -\frac{sP_{TX}G_i}{mX_L r^{\alpha_L/2}}) - 1)\right]\right), \end{aligned} \quad (20)$$

where ${}_2F_1$ denotes the Gauss hypergeometric function. The Laplace transform for the NLoS can be derived substituting the appropriate path loss parameters.

The total interference is given then by:

$$L_I^{mmWave}(s) = L_{I,L}^{mmWave}(s) + L_{I,NL}^{mmWave}(s). \quad (21)$$

In Table 2 it can be seen that for the 28 GHz mmWave frequency $\alpha_L = 2$ represents a common value. This has a reason also in the fact the for $\alpha_L = 2$ the Gauss hypergeometric function can be simplified using its series expansion [17].

E. OUTAGE PROBABILITY AND SPECIAL CASES

Considering the above derivations, it follows the final outage probability for a FH to a UAV-DU for both the sub-6 GHz and the mmWave case. Deriving the final expression of the outage probability from (8) involves the intermediate steps of considering the conditional coverage probability given that the tagged BS is LoS or NLoS, as seen from the reference UAV at origin.

Proposition 1: Given that the UAV-DU is fronthauled by a LoS/NLoS terrestrial BS at a distance R_ω , $\omega \in \{L, NL\}$, and Nakagami- m fading, we generalize the expression of the conditioned coverage probability with an SINR threshold Γ as:

$$\begin{aligned} &(p_{F,cov|r}^\omega(\lambda, \Gamma)) \\ &= P\left[f > \frac{\Gamma(I + \sigma_n^2)}{P_{TX}l^\omega(R_\omega)G} | R_\omega = r\right] \\ &\approx \sum_{n=1}^m (-1)^{n+1} \binom{m}{n} \int_{h_{diff}}^\infty \exp\left(-\frac{n\eta\Gamma\sigma_n^2}{P_{TX}G_0l^\omega(r)}\right) \\ &\quad \times L_I\left(\frac{n\eta\Gamma}{P_{TX}Gl^\omega(r)}\right) f_{R_\omega}(r) dr \end{aligned} \quad (22)$$

where f_{R_ω} is the PDF of R_ω , m is the fading Nakagami shape parameter, $\eta = m(m!)^{-\frac{1}{m}}$ and L_I the Laplace functional of the interference I .

It is necessary then to multiply the conditional coverage probabilities given that the UAV-DU is associated with a LoS or a NLoS BS with the probability that the UAV-DU is associated with a LoS or NLoS BS, P_{AL} and P_{ANL} , respectively (13):

$$\begin{aligned} P_{out}(SINR < \Gamma) &= 1 - P_{cov}(SINR > \Gamma) \\ &= 1 - [p_{F,cov|r}^L(\lambda, \Gamma)P_{AL} + p_{F,cov|r}^{NL}(\lambda, \Gamma)(1 - P_{AL})]. \end{aligned} \quad (23)$$

We note that (22) can be straightforward used for the sub-6 GHz case inserting the Laplace transform of interference expression formulated in (18). For the mmWave case, if the step probability function (2) is considered, the final outage probability can be derived utilizing the upper bound in (4) and a successive Gaussian-Chebyshev quadrature equation [17] (see Appendix E). Given the consideration on the continuity of (3), we can conclude the derivation substituting (21) in (22).

The expressions in (22) generally involve numerical evaluations of multiple integrals and may become difficult to analyze. We simplify the analysis for two cases where specific conditions occur. The validity of these conditions will be investigated in the simulation section.

1) OUTAGE PROBABILITY IN LoS CONDITIONS

Case 1: Increasing the operational altitude of the UAV-DU, it is very likely that the link to the terrestrial BS is purely LoS. The LoS probability in (3) can be approximated ignoring the NLoS contribution.

In the case the ground-to-air link is purely LoS, we can ignore the NLoS contribution and the conditioned coverage probability becomes:

$$\begin{aligned} &p_{F,cov|r}^L(\lambda, \Gamma) \\ &\approx \sum_{n=1}^m (-1)^{n+1} \binom{m}{n} \int_{h_{diff}}^\infty \exp\left(-\frac{n\eta\Gamma\sigma_n^2}{P_{TX}G_0l^L(r)}\right) \\ &\quad \times L_I\left(\frac{n\eta\Gamma}{P_{TX}Gl^L(r)}\right) f_{R_L}(r) dr. \end{aligned} \quad (24)$$

2) OUTAGE PROBABILITY IN INTERFERENCE LIMITED NETWORKS

Case 2: In this case, we investigate the network performance metrics when the interference is negligible. With large bandwidth and high directionality, not extremely dense deployed mmWave networks tend to be noise limited [15]. In the above conditions, we can consider interference has a negligible effect on the single UAV-DU FH link under analysis and it can be considered noise limited.

When the interference is negligible, we can consider that $L(\cdot) = 1$. The conditioned coverage probability (22) becomes then:

$$p_{cov|r}^\omega(\lambda, \Gamma) \approx \sum_{n=1}^m (-1)^{n+1} \binom{m}{n} \int_{h_{diff}}^{\infty} \exp\left(-\frac{n\eta\Gamma\sigma_n^2}{P_{TX}G_0l^\omega(r)}\right) f_{R_\omega}(r) dr. \quad (25)$$

3) TARGET RATE ANALYSIS

In this section, we define a rate outage probability as the figure of merit to determine the reliability of the considered FH link [15]. The rate outage represents the probability that the rate of the FH link falls below a certain threshold R_{FH} . In general, the FH rate requirement is given by the synchronization and processing samples between the CU and the DU. There are multiple candidates for splitting processing between the CU and the DU, that lead to different processing power and rate requirements. This is usually referred as functional split. The discussion on the details of the different splits is not the objective of this paper, and we refer the interested readers to [3] and [28]. Here, we consider that with more baseband functions at the UAV-DU the rate FH requirement is lower and depends on the load of the network, e.g. the utilization of the subcarriers, than the antenna elements [28]. A lower protocol split, on the other hand, scales the overhead with the number of antennae and sampling frequency.

In addition, the data rate in the access link between the UAV and the UEs depends on the available capacity on the FH network. Given a FH rate of R_{FH} , the total amount of data available on the access link is given by $R_{AL} = R_{FH}/x$, where x is the quantity of resources utilized for the FH overhead and transport.

Accordingly with these factors, we consider initially a higher protocol stack split, where the transport data rate approximately follows the data rate experienced by the user ($x \approx 1$) and we investigate which technology minimize the outage probability given an average data rate on the access link. Secondly, as it will be seen in subsection IV-C, we investigate the general impact of a lower protocol stack split when the number of antennae increases at the BS to exploit a greater beamforming gain.

Having determined the target rate R_{FH} , the rate outage can be obtained than as:

$$P_{R,out}(Rate < \Gamma_r) = 1 - [p_{F,cov|r}^L(\lambda, \Gamma_r)P_{AL} + p_{F,cov|r}^{NL}(\lambda, \Gamma_r)(1 - P_{AL})], \quad (26)$$

where $\Gamma_r = 2^{R_{FH}/B} - 1$ and B is the bandwidth.

IV. NUMERICAL RESULTS AND DISCUSSION

In this section we show the numerical results for the outage probability expressions derived above. Table 3 summarizes the parameters used for the mmWave simulations, unless referred otherwise. The corresponding parameters for the sub-6 GHz simulations are the same except done for the antenna gain, path loss and fading parameters. We adopt the sub-6 GHz parameters commonly used in literature [10], [16]: omnidirectional antennae at the UAV, 43 dBm in transmission at the BS, $\alpha_L = 2$, $\alpha_{NL} = 3.5$ and it is assumed Rayleigh fading ($m = 1$) for NLoS transmission. It is not required any change for the LoS probability. DUs are lighter and less complex than the BS, due to the simpler RF and cooling system. Depending on several parameters, such as the number of bands deployed and the transmission power, their weight is typically up to few kilograms [29]. For this reason, we consider for our simulations UAVs able to cope with that payload. Recent UAVs categorizations [4], [30] mention that multi-rotor of small/medium size fall into this category. Hence, we can consider altitudes up to hundreds meters, subject to the local aviation regulations of operations.

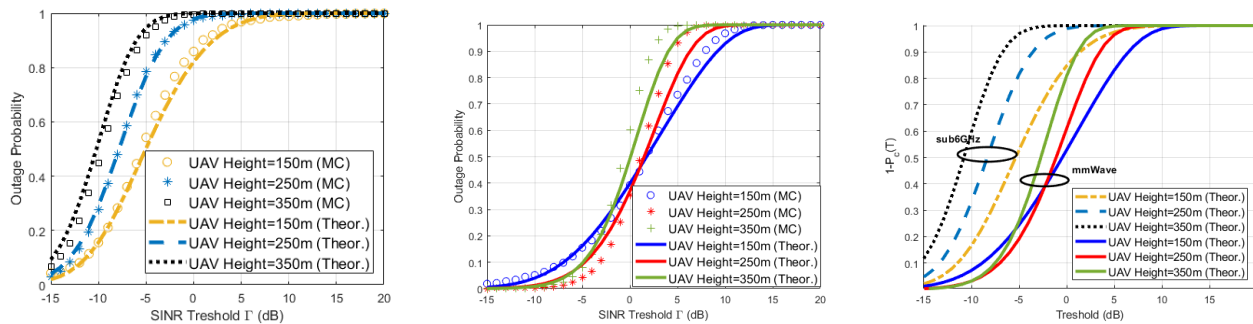
TABLE 3. Simulation parameters.

Parameters	Value	Value
Carrier Frequency (f_C)	28 GHz	70 GHz
Path Loss LoS (α_L)	2	2.25 [17]
Path Loss NLoS (α_{NL})	4	3.76 [17]
Number of antennae (N)	UAV= 4, BS = 8	UAV= 4, BS = 8-144
Bandwidth (B)	100 MHz	500 MHz
Noise (σ_n^2)	$4 \cdot 10^{-10}$	$4 \cdot 10^{-10}$
Ground BS height	19-25 m	19-25 m
Ground BS Power (P_{TX})	10 W [17]	10 W [16]
Number of MC runs	10^4	10^4

A. EVALUATION AND IMPACT OF NLoS

In this section, we utilize Monte Carlo (MC) simulations to validate the accuracy of the analytical expressions derived in the previous section. Fig. 4 shows the validation of Proposition 1 for both the sub-6 GHz (2 GHz) and mmWave (28 GHz) band in a dense urban scenario, represented by a terrestrial density of $5/(250^2\pi)$, and a , b and c as for the Urban case in [14, Table 1]. The number of antenna elements, and as a consequence the linear gain, is 4 at the UAV-DU, while 8 at the terrestrial BS. We set to zero the gain of the sidelobes. As for Case 2, we focus on finding the outage distribution in a network with negligible interference effects. The UAV is flying at altitude between 150 m-350 m. As it is visible, the outage probability derived using the expressions in (23) match the MC simulations with a good approximation. For all cases, the outage probability increase with the increase of the SINR threshold. The mmWave case is outperforming over the sub-6 GHz.

The effect of changing the environment of the blockage model for different UAV heights and the contribution of the NLoS transmissions is shown in Fig. 5 for the mmWave. The building environment can be modified from a more dense



(a) Outage probability versus the SINR for the sub-6 GHz band (b) Outage probability versus the SINR for the mmWave band (c) Comparison of sub-6 GHz and mmWave outage probability versus SINR

FIGURE 4. Given a terrestrial BS density of $5/(250^2\pi)m^{-2}$, figures (a), (b) show the match of Monte Carlo Simulations with Analytical Results for the sub-6 GHz band and mmWave, respectively. In (c) we compare the outage probability of both the frequency bands.

to a sparse one changing the inter-site distance between the building, λ and their characteristics, parameter b in (3). In a dense environment, as it can be seen in Fig. 5, considering only the LoS transmission in the outage probability is not accurate when the UAV height is low, where the NLoS components for an urban environment is stronger. Increasing the UAV height, ignoring the NLoS contribution provides accurate results and confirm the validation of the approximation in Case 1. When the building environment change to a more sparse one ($\lambda = 1/(250^2)\pi$, $b = 6.581$) Case 1 is validated also at low UAV height.

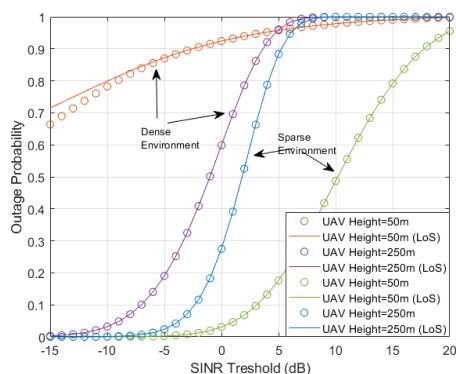


FIGURE 5. mmWave fronthaul outage versus the SINR threshold for different BS densities.

B. OUTAGE ANALYSIS FOR A TARGET FH RATE

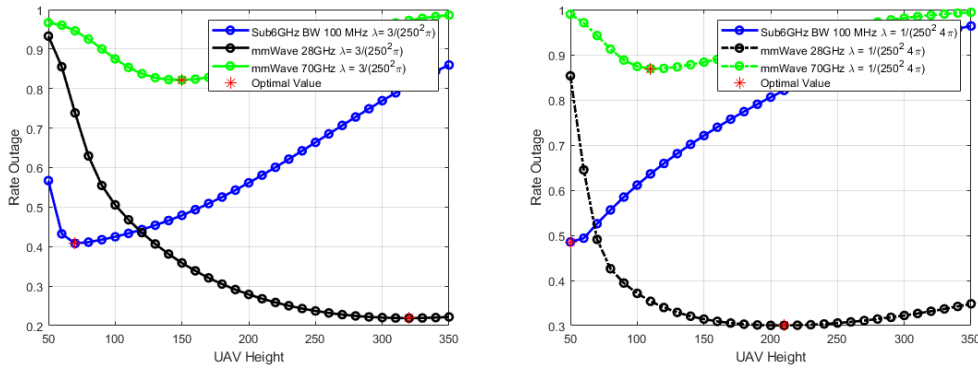
We have shown that at high UAV altitudes, LoS transmissions are dominant over the NLoS, potentially a beneficial situation for a mmWave link. However, a greater distance from the connected BS also increase the path loss as for (1), and this effect might have an impact with the increase of the operating frequency. We are now interested in investigating the optimal altitude that minimizes the outage probability. We focus on three possible 5G enabler bands: sub-6 GHz at 3.5 GHz, a mmWave link at 28 GHz and a mmWave link at 70 GHz. To overcome the rapid saturation of the sub-6 GHz resources,

at the carrier frequency of 3.5 GHz it is possible to aggregate five contiguous component carriers of 20 MHz each for a total of 100 MHz [31]. The 28 GHz and 70 GHz mmWave bands have 100 MHz and 1 GHz, respectively. For all remaining 70 GHz parameters the reader should refer to Table 3.

We consider to establish a FH link to a UAV-DU in order to satisfy typical emergency services on the access link, with traffic demands for user varying from 720 Kbps to 1 Mbps, and a total access rate depending on the number of served UEs [32]. We fix the corresponding SINR threshold for each frequency band enough to satisfy a total average downlink rate in the access link of 45 Mbps. Fig. 6 shows the outage probability versus the UAV height for different building densities. An optimal value of height minimizes the outage probability for each frequency band. There are three major observations: First, the path loss has a prominent role increasing the frequency of the mmWave band. At low mmWave frequencies, e.g. 28 GHz, due to the better path loss exponent and intercepts, the outage probability is lower than at higher mmWave frequencies. Second, a lower BS density improves the outage probability (Fig. 6b). On the other hand, the optimal height is higher in a dense environment. At last, at low heights, where the NLoS has a higher impact on the performance of the FH link, the sub-6 GHz is outperforming the mmWave bands, due to its less sensitivity to blockage.

C. EFFECT OF THE ANTENNA GAIN AND SPLIT COMPARISON

In Fig. 7 we focus our attention on the impact of the antenna gain at mmWave band for a fixed BS density. Higher carrier frequencies allow more antenna elements to be deployed at the transceiver [17]. For this reason, we consider to deploy up to 144 antenna elements at 70 GHz. To keep the complexity and the energy consumption low at the UAV it is possible to change the number of the antenna elements at the terrestrial BS only. Fig. 7 shows the direct effect on the main lobe gain to counteract the higher path losses at high frequencies. Exploiting the large bandwidth that mmWave has to offer with high directional antennae, the overall rate



(a) Rate Outage probability versus the UAV height, (b) Rate Outage probability versus the UAV height, with $\lambda = 3/(250^2 \pi)$ with $\lambda = 1/(250^2 4 \pi)$

FIGURE 6. Rate outage probability for sub-6 GHz and mmWave band for different terrestrial densities and a rate, without min threshold.

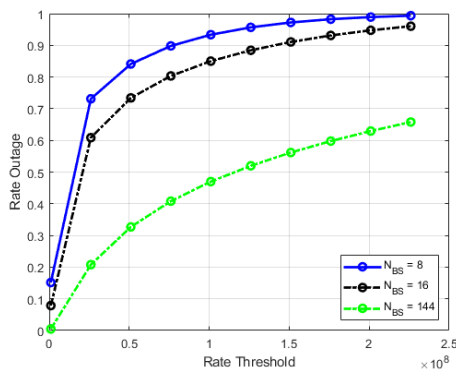


FIGURE 7. Effect of antenna gain on the rate outage probability for BS density of $\lambda = 3/(250^2 \pi)$.

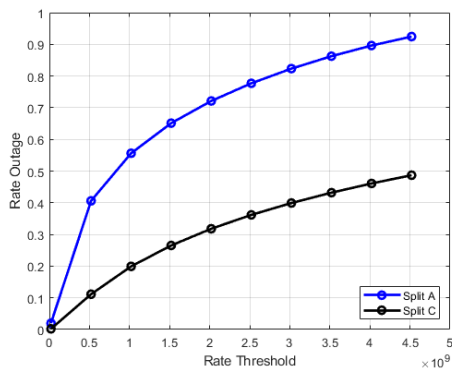


FIGURE 8. Effect of splitting the protocol stack at lower level on a 500 MHz FH link at 70 GHz.

outage decrease significantly. However, in a FH link, this come at a cost when considering different split options at the FH. We consider a split at the RF, split A, and a split C, where only higher MAC-layer functionalities (e.g., scheduling) are centralized. Fig. 8 shows the effect of splitting the protocol stack of the FH link at lower layer when 144 antenna elements are deployed at the ground BS. The overhead x is increasing with the number of antennae accordingly as the normalized peak values of [28, Table 1].

V. CONCLUSION AND FUTURE WORK

In this paper we have presented an analytical model to study the outage probability of a FH link to a UAV-DU. We have derived the approximated outage expression for a mmWave FH link. Overall, mmWave networks provide a FH with a minor outage probability compared to a sub-6 GHz. For longer distances and sparse terrestrial BS density, the direct FH link shows an overall performance deterioration for both bands. In addition, our results show that mmWave networks can be assisted by sub-6 GHz to decrease the outage probability, especially at low UAV heights, where the blockage has a higher impact on the performance of the FH link. This motivates us to consider, in future works, an intelligent band switching algorithm with the use of machine learning techniques to increase the reliability of the FH link.

This work can be extended in a number of directions. It would be beneficial to include in the network analysis access link and a hybrid beamforming Multiple Input Multiple Output (MIMO) terrestrial network. This could provide insights on the impact of network parameters, such as the number of RF chains, on the FH performance with different protocol splits. Allowing a multi-hop FH link in sparser deployment of terrestrial BSs could also be investigated in future work.

APPENDIX A SERVING DISTANCE

Similarly to [14], the CCDF of the random distance R between the UAV and the closest LoS/NLoS ground BS can be written as:

$$CCDF_R(r) = P(R > r) \stackrel{(a)}{=} \exp\left(-2\pi\lambda \int_{h_{diff}}^r P_\omega(t)tdt\right), \tag{A-1}$$

where (a) comes from the null probability of the PPP, $\omega \in \{LoS, NLoS\}$ and t is a dummy variable. Note that $P_{LoS}(z)$ can be expressed as function of the distance r , considering that

$z = \sqrt{r^2 - h_{diff}^2}$, with $r \geq h_{diff}$. With a change of variable in the integral with respect to z and considering $f_R(r) = \frac{dF_R(r)}{dr}$, we get (9) and (10).

APPENDIX B PROOF OF LEMMA 3

$$\begin{aligned} P_{A_L} &= P\left(X_L R_L^{-\alpha_L} > X_{NL} R_{NL}^{-\alpha_{NL}}\right) \\ &= P\left(R_{NL} > \left(\frac{X_{NL}}{X_L} R_L^{\alpha_L}\right)^{\frac{1}{\alpha_{NL}}}\right). \end{aligned} \quad (\text{B-1})$$

Conditioning for $R_L = r$ and considering $\left(\frac{X_{NL}}{X_L} r^{\alpha_L}\right)^{\frac{1}{\alpha_{NL}}} = r_{I,NL}$ we obtain:

$$\begin{aligned} &\int_{h_{diff}}^{\infty} P(R_{NL} > r_{I,NL} | R_L = r) f_{R_L}(t) dt \\ &\stackrel{(a)}{=} \int_{h_{diff}}^{\infty} (1 - F_{R_{NL}}(r_{I,NL})) f_{R_L}(t) dt \\ &\stackrel{(b)}{=} \int_{h_{diff}}^{\infty} \left(\exp\left(-2\pi\lambda \int_{h_{diff}}^{r_{I,NL}} t P_{NLoS}(\sqrt{t^2 - h_{diff}^2}) dt\right) \right) f_{R_L}(t) dt, \end{aligned} \quad (\text{B-2})$$

where (a) comes from the definition of CDF and (b) from (A-1).

APPENDIX C LAPLACE INTERFERENCE DERIVATION

If the LoS probability in equation (2) is considered, the integral in the exponent of (19) can be substituted with a weighted sum of integrals [11]. Equation (C-1), as shown at the bottom of this page, shows the expression for the LoS case, where γ is defined in II-A. P_{LoS} and the integral are evaluated with step $1/\sqrt{\beta_1\beta_2}$, where β_1, β_2 are defined in II-A. Equation (C-2), as shown at the bottom of this page, shows the derivation of a closed-form expression for the integral $\int_a^b (1 - (1 + \frac{sP_{TX}GX_k}{mr^{\alpha_k}})^{-m}) r dr$, where k generalize the derivation for the NLoS case also. In (a) we applied the substitution $y = r^{\alpha_k}$ and (b) comes from applying [11, (c)-(d) (11)] where ${}_2F_1$ denotes the Gauss hypergeometric function. Using this final expression for the integral in (C-1) and substituting G with the antenna gain of the interference links G_i as for the antenna model concludes the derivation. The final expression of the Laplace interference for the LoS case is in (C-3), as shown at the bottom of this page, where $\zeta_m^L(\cdot)$ is a compact representation of the integral in (C-2). The Laplace transform for the NLoS interferers is solved starting from (C-1) and (C-2) and substituting α_L, X_L with α_{NL}, X_{NL} .

$$\begin{aligned} L_{I,L}^{mmWave}(s) &= \exp\left(-2\pi\lambda \int_r^{\infty} (1 - E_G[(1 + \frac{sP_{TX}GX_L}{mr^{\alpha_L}})^{-m}]) P_{LoS}(\sqrt{t^2 - h_{diff}^2}) dt\right) \\ &= \exp\left(-2\pi\lambda E_G\left[\int_r^{r+1/\sqrt{\beta_1\beta_2}} (1 - (1 + \frac{sP_{TX}GX_L}{mr^{\alpha_L}})^{-m}) P_{LoS}(\sqrt{\gamma^2 - h_{diff}^2}) r dr\right.\right. \\ &\quad \left.\left.+ \sum_{j=\gamma+1}^{\infty} \int_{j/\sqrt{\beta_1\beta_2}}^{(j+1)/\sqrt{\beta_1\beta_2}} (1 - (1 + \frac{sP_{TX}GX_L}{mr^{\alpha_L}})^{-m}) P_{LoS}(\sqrt{j^2 - h_{diff}^2}) r dr\right]\right) \end{aligned} \quad (\text{C-1})$$

$$\begin{aligned} &\int_a^b \left(1 - \left(1 + \frac{sP_{TX}GX_k}{mr^{\alpha_k}}\right)^{-m}\right) r dr \\ &= \int_a^b \left(1 - \left(\frac{mr^{\alpha_k}}{mr^{\alpha_k} + sP_{TX}GX_k}\right)^m\right) r dr \\ &\stackrel{(a)}{=} \frac{1}{\alpha_k} \int_{a^{\alpha_k}}^{b^{\alpha_k}} \left(1 - \left(\frac{my}{my + sP_{TX}GX_k}\right)^m\right) y^{2/\alpha_k - 1} dy \\ &\stackrel{(b)}{=} \sum_{i=1}^m (-1)^{i+1} \binom{m}{i} \left(\frac{b^2}{2} {}_2F_1\left(i, \frac{2}{\alpha_k}; 1 + \frac{2}{\alpha_k}; -\frac{mb^{\alpha_k}}{sP_{TX}GX_k}\right) - \frac{a^2}{2} {}_2F_1\left(i, \frac{2}{\alpha_k}; 1 + \frac{2}{\alpha_k}; -\frac{ma^{\alpha_k}}{sP_{TX}GX_k}\right)\right) \end{aligned} \quad (\text{C-2})$$

$$\begin{aligned} L_{I,L}^{mmWave}(s|D) &= \exp\left(-2\pi\lambda E_G\left[\zeta_m^L(s, r, \frac{\gamma+1}{\sqrt{\beta_1\beta_2}}, G) P_{LoS}(\sqrt{\gamma^2 - h_{diff}^2}) + \sum_{j=\gamma+1}^{\infty} \zeta_m^L(s, \frac{j}{\sqrt{\beta_1\beta_2}}, \frac{j+1}{\sqrt{\beta_1\beta_2}}, G) P_{LoS}(\sqrt{j^2 - h_{diff}^2})\right]\right) \\ &= \exp\left(-2\pi\lambda \sum_{i=1}^4 p_i \left[\zeta_m^L(s, r, \frac{\gamma+1}{\sqrt{\beta_1\beta_2}}, G_i) P_{LoS}(\sqrt{\gamma^2 - h_{diff}^2}) + \sum_{j=\gamma+1}^{\infty} \zeta_m^L(s, \frac{j}{\sqrt{\beta_1\beta_2}}, \frac{j+1}{\sqrt{\beta_1\beta_2}}, G_i) P_{LoS}(\sqrt{j^2 - h_{diff}^2})\right]\right) \end{aligned} \quad (\text{C-3})$$

The adoption of the approximated version of the LoS probability (3) let us directly apply the property of the integral $\int_N^\infty (1 - (1 + sy^{-\alpha})^{-m})ydy = N^2/2({}_2F_1(-2/\alpha, m; 1 - 2/\alpha; -s/N^\alpha))$ [17] to the integral in (19), leading to:

$$\begin{aligned}
 L_{I,L}^{mmWave}(s|D) &= \exp\left(-2\pi\lambda \int_r^\infty (1 - E_G[(1 + \frac{sP_{TX}GX_L}{mr^{\alpha_L/2}})^m]) \right. \\
 &\quad \left. \times P_{LoS}(\sqrt{t^2 - h_{diff}^2})tdt\right) \\
 &= \exp\left(-2\pi\lambda P_{LoS}(\sqrt{r^2 - h_{diff}^2}) \right. \\
 &\quad \left. \times E_G\left[\frac{r^2}{2}({}_2F_1(-\frac{2}{\alpha_L}, m; 1 - \frac{2}{\alpha_L}; -\frac{sP_{TX}GX_L}{mr^{\alpha_L}}) - 1)\right]\right). \tag{C-4}
 \end{aligned}$$

Substituting the expectation of the interference gain as for the antenna model in Section II-D concludes the derivation:

$$\begin{aligned}
 L_{I,L}^{mmWave}(s|D) &= \exp\left(-2\pi\lambda P_{LoS}(\sqrt{r^2 - h_{diff}^2}) \right. \\
 &\quad \left. \sum_{i=1}^4 p_i \left[\frac{r^2}{2}({}_2F_1(-\frac{2}{\alpha_L}, m; 1 - \frac{2}{\alpha_L}; -\frac{sP_{TX}G_iX_L}{mr^{\alpha_L}}) - 1)\right]\right). \tag{C-5}
 \end{aligned}$$

For the NLoS case, we obtain:

$$\begin{aligned}
 L_{I,NL}^{mmWave}(s|D) &= \exp\left(-2\pi\lambda P_{NLoS}(\sqrt{r^2 - h_{diff}^2}) \right. \\
 &\quad \left. \sum_{i=1}^4 p_i \left[\frac{r^2}{2}({}_2F_1(-\frac{2}{\alpha_{NL}}, m; 1 - \frac{2}{\alpha_{NL}}; -\frac{sP_{TX}G_iX_{NL}}{mr^{\alpha_{NL}}}) - 1)\right]\right). \tag{C-6}
 \end{aligned}$$

**APPENDIX D
PROOF OF PROPOSITION 1**

In (D-1), as shown at the bottom of this page, we provide the proof for a UAV-DU connected to a LoS BS. Same steps can be followed for the NLoS case. Step (a) comes from (4) while (b) follows from Binomial theorem, the assumption that m is integer and the linearity of expectation. In (c) we calculated the average antenna gain is G_0 for the reference UAV-DU and denoted the Laplace functional of the interference as $L_I(s) = E[\exp(-sI)]$.

**APPENDIX E
COVERAGE PROBABILITY DERIVATION**

In (E-1), as shown at the bottom of this page, we have derived the conditioned coverage probability when (2) is applied from (22). In (E-1) $\omega \in \{L, NL\}$, β_1, β_2 are the LoS probability parameters in (2), (a) comes from the step property of (2), (b) comes from [17, Appendix B.2-(d)]. Expression $\rho = \cos(\pi \frac{2k-1}{2m})$, with $k = \{1, 2, \dots, M\}$ denotes

$$\begin{aligned}
 (p_{F,cov|r}^L(\lambda, \Gamma)) &= P\left[f > \frac{\Gamma(I + \sigma_n^2)}{P_{TX}G_I^L(R_L)} | R_L = r\right] = \int_{h_{diff}}^\infty \left(P\left[f > \frac{\Gamma(I + \sigma_n^2)}{P_{TX}G_I^L(r)}\right]\right) f_{R_L}(r)dr \\
 &\stackrel{(a)}{\approx} \int_{h_{diff}}^\infty \left(1 - E\left[\left(1 - \exp\left(-\frac{n\eta\Gamma(I + \sigma_n^2)}{P_{TX}G_I^L(r)}\right)\right)^m\right]\right) f_{R_L}(r)dr \\
 &\stackrel{(b)}{=} \sum_{n=1}^m (-1)^{n+1} \binom{m}{n} \int_{h_{diff}}^\infty E\left[\exp\left(-\frac{\eta\Gamma\sigma_n^2}{P_{TX}G_I^L(r)}\right)\right] E\left[\exp\left(-\frac{\eta\Gamma I}{P_{TX}G_I^L(r)}\right)\right] f_{R_L}(r)dr \\
 &\stackrel{(c)}{=} \sum_{n=1}^m (-1)^{n+1} \binom{m}{n} \int_{h_{diff}}^\infty \left(\left[\exp\left(-\frac{n\eta\Gamma\sigma_n^2}{P_{TX}G_0I^L(r)}\right)\right] L_I\left(\frac{n\eta\Gamma}{P_{TX}G_I^L(r)}\right)\right) f_{R_L}(r)dr, \tag{D-1}
 \end{aligned}$$

$$\begin{aligned}
 (p_{F,cov|r}^\omega(\lambda, \Gamma)) &\approx \sum_{n=1}^m (-1)^{n+1} \binom{m}{n} \int_{h_{diff}}^\infty \exp\left(-\frac{n\eta\Gamma\sigma_n^2}{P_{TX}G_0I^\omega(r)}\right) L_I\left(\frac{n\eta\Gamma}{P_{TX}G_I^\omega(r)}\right) f_{R_\omega}(r)dr \\
 &\stackrel{(a)}{\approx} \sum_{\gamma \in Z^*} \sum_{n=1}^m (-1)^{n+1} \binom{m}{n} \int_{\frac{\gamma}{\sqrt{\beta_1\beta_2}}}^{\frac{\gamma+1}{\sqrt{\beta_1\beta_2}}} \exp\left(-\frac{n\eta\Gamma\sigma_n^2}{P_{TX}G_0I^\omega(r)}\right) L_I\left(\frac{n\eta\Gamma}{P_{TX}G_I^\omega(r)}\right) f_{R_\omega}(r)dr \\
 &\stackrel{(b)}{=} \frac{\pi}{2M\sqrt{\beta_1\beta_2}} \sum_{k=1}^M \sqrt{1 - \rho^2} \sum_{\gamma \in Z^*} \left(\sum_{n=1}^m (-1)^{n+1} \binom{m}{n} \exp\left(-\frac{n\eta\Gamma\sigma_n^2}{P_{TX}G_0I^\omega(r)}\right) L_I\left(\frac{n\eta\Gamma}{P_{TX}G_I^\omega(r)}\right) f_{R_\omega}(r)\right) \tag{E-1}
 \end{aligned}$$

the Gauss-Chebyshev node, where M is the parameter balancing the accuracy and the complexity. Z^* is the infinite range of non-negative integers, but only the first three values (0,1,2) can be used without affecting the performance of the analysis [17].

ACKNOWLEDGEMENT

The authors would like to thank Mr. Brian Keogh of the University of College Dublin for his comments on drafts of this work. They also thank the Editor and anonymous reviewers for their constructive comments.

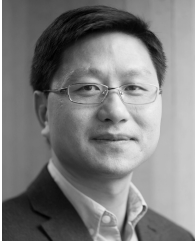
REFERENCES

- [1] Y. Zeng, R. Zhang, and T. J. Lim, "Wireless communications with unmanned aerial vehicles: Opportunities and challenges," *IEEE Commun. Mag.*, vol. 54, no. 5, pp. 36–42, May 2016.
- [2] A. Ghosh, A. Maeder, M. Baker, and D. Chandramouli, "5G evolution: A view on 5G cellular technology beyond 3GPP release 15," *IEEE Access*, vol. 7, pp. 127639–127651, 2019.
- [3] L. M. P. Larsen, A. Checko, and H. L. Christiansen, "A survey of the functional splits proposed for 5G mobile crosshaul networks," *IEEE Commun. Surveys Tuts.*, vol. 21, no. 1, pp. 146–172, 1st Quart., 2019.
- [4] H. Ahmadi, K. Katzis, and M. Z. Shakir, "A novel airborne self-organising architecture for 5G+ networks," in *Proc. IEEE 86th Veh. Technol. Conf. (VTC-Fall)*, Sep. 2017, pp. 1–5.
- [5] M. R. Akdeniz, Y. Liu, M. K. Samimi, S. Sun, S. Rangan, T. S. Rappaport, and E. Erkip, "Millimeter wave channel modeling and cellular capacity evaluation," *IEEE J. Sel. Areas Commun.*, vol. 32, no. 6, pp. 1164–1179, Jun. 2014.
- [6] J. G. Andrews, A. K. Gupta, and H. S. Dhillon, "A primer on cellular network analysis using stochastic geometry," 2016, *arXiv:1604.03183*. [Online]. Available: <http://arxiv.org/abs/1604.03183>
- [7] I. Atzeni, J. Arnau, and M. Kountouris, "Downlink cellular network analysis with LOS/NLOS propagation and elevated base stations," *IEEE Trans. Wireless Commun.*, vol. 17, no. 1, pp. 142–156, Jan. 2018.
- [8] M. Mozaffari, W. Saad, M. Bennis, and M. Debbah, "Unmanned aerial vehicle with underlaid device-to-device communications: Performance and tradeoffs," *IEEE Trans. Wireless Commun.*, vol. 15, no. 6, pp. 3949–3963, Jun. 2016.
- [9] A. Al-Hourani, S. Kandeepan, and S. Lardner, "Optimal LAP altitude for maximum coverage," *IEEE Wireless Commun. Lett.*, vol. 3, no. 6, pp. 569–572, Dec. 2014.
- [10] M. Alzenad and H. Yanikomeroglu, "Coverage and rate analysis for unmanned aerial vehicle base stations with LoS/NLoS propagation," in *Proc. IEEE Globecom Workshops (GC Wkshps)*, Dec. 2018, pp. 1–7.
- [11] B. Galkin, J. Kibilda, and L. A. DaSilva, "Coverage analysis for low-altitude UAV networks in urban environments," in *Proc. IEEE Global Commun. Conf. (GLOBECOM)*, Dec. 2017, pp. 1–6.
- [12] D. López-Pérez, M. Ding, H. Li, L. G. Giordano, G. Geraci, A. Garcia-Rodriguez, Z. Lin, and M. Hassan, "On the downlink performance of UAV communications in dense cellular networks," in *Proc. IEEE Global Commun. Conf. (GLOBECOM)*, Dec. 2018, pp. 1–7.
- [13] M. Alzenad and H. Yanikomeroglu, "Coverage and rate analysis for vertical heterogeneous networks (VHetNets)," *IEEE Trans. Wireless Commun.*, vol. 18, no. 2, pp. 5643–5657, Dec. 2019, doi: [10.1109/TWC.2019.2938168](https://doi.org/10.1109/TWC.2019.2938168).
- [14] N. Cherif, M. Alzenad, H. Yanikomeroglu, and A. Yongacoglu, "Downlink coverage and rate analysis of an aerial user in integrated aerial and terrestrial networks," 2019, *arXiv:1905.11934*. [Online]. Available: <http://arxiv.org/abs/1905.11934>
- [15] J. G. Andrews, T. Bai, M. N. Kulkarni, A. Alkhateeb, A. K. Gupta, and R. W. Heath, Jr., "Modeling and analyzing millimeter wave cellular systems," *IEEE Trans. Commun.*, vol. 65, no. 1, pp. 403–430, Jan. 2017.
- [16] B. Galkin, J. Kibilda, and L. A. DaSilva, "Backhaul for low-altitude UAVs in urban environments," in *Proc. IEEE Int. Conf. Commun. (ICC)*, May 2018, pp. 1–6.
- [17] W. Yi, Y. Liu, E. Bodanese, A. Nallanathan, and G. K. Karagiannidis, "A unified spatial framework for UAV-aided mmWave networks," *IEEE Trans. Commun.*, vol. 67, no. 12, pp. 8801–8817, Dec. 2019.
- [18] *Technical Specification Group Radio Access Network; Study on Enhanced LTE Support for Aerial Vehicles (Release 15)*, document TR 36.777, 3GPP, Dec. 2017.
- [19] W. Yi, Y. Liu, M. Elkashlan, and A. Nallanathan, "Modeling and coverage analysis of downlink UAV networks with mmWave communications," in *Proc. IEEE Int. Conf. Commun. Workshops (ICC Workshops)*, May 2019, pp. 1–6.
- [20] X. Wang and M. C. Gursoy, "Coverage analysis for energy-harvesting UAV-assisted mmWave cellular networks," *IEEE J. Sel. Areas Commun.*, vol. 37, no. 12, pp. 2832–2850, Dec. 2019.
- [21] *Propag. Data and Prediction Methods Required for the Design of Terrestrial Broadband Radio Access Systems Operating in a Frequency Range From 3 to 60 GHz*, document ITU-R Recommendation P.1410-5, 2012.
- [22] J. Holis and P. Pechac, "Elevation dependent shadowing model for mobile communications via high altitude platforms in built-up areas," *IEEE Trans. Antennas Propag.*, vol. 56, no. 4, pp. 1078–1084, Apr. 2008.
- [23] T. Bai and R. W. Heath, Jr., "Coverage and rate analysis for millimeter-wave cellular networks," *IEEE Trans. Wireless Commun.*, vol. 14, no. 2, pp. 1100–1114, Feb. 2015.
- [24] V. Va, T. Shimizu, G. Bansal, and R. W. Heath, Jr., "Online learning for position-aided millimeter wave beam training," *IEEE Access*, vol. 7, pp. 30507–30526, 2019.
- [25] M. Taghi Dabiri, H. Safi, S. Parsaeefard, and W. Saad, "Analytical channel models for millimeter wave UAV networks under hovering fluctuations," 2019, *arXiv:1905.01477*. [Online]. Available: <http://arxiv.org/abs/1905.01477>
- [26] H.-S. Jo, Y. J. Sang, P. Xia, and J. G. Andrews, "Heterogeneous cellular networks with flexible cell association: A comprehensive downlink SINR analysis," *IEEE Trans. Wireless Commun.*, vol. 11, no. 10, pp. 3484–3495, Oct. 2012.
- [27] V. Vardhan Chetlur and H. S. Dhillon, "Downlink coverage analysis for a finite 3-D wireless network of unmanned aerial vehicles," *IEEE Trans. Commun.*, vol. 65, no. 10, pp. 4543–4558, Oct. 2017.
- [28] J. Bartelt, N. Vucic, D. Camps-Mur, E. Garcia-Villegas, I. Demirkol, A. Fehske, M. Grieger, A. Tzanakaki, J. Gutiérrez, E. Grass, G. Lyberopoulos, and G. Fettweis, "5G transport network requirements for the next generation fronthaul interface," *EURASIP J. Wireless Commun. Netw.*, vol. 2017, no. 1, p. 89, May 2017.
- [29] W. Honcharenko, "Sub-6 GHz mMIMO base stations meet 5G's size and weight challenges," *Microw. J.*, vol. 62, no. 2, pp. 40–52, 2019.
- [30] A. Fotouhi, H. Qiang, M. Ding, M. Hassan, L. G. Giordano, A. Garcia-Rodriguez, and J. Yuan, "Survey on uav cellular communications: Practical aspects, standardization advancements, regulation, and security challenges," *IEEE Commun. Surveys Tuts.*, vol. 21, no. 4, pp. 3417–3442, 4th Quart., 2019, doi: [10.1109/COMST.2019.2906228](https://doi.org/10.1109/COMST.2019.2906228).
- [31] Z. Khan, H. Ahmadi, E. Hossain, M. Coupechoux, L. A. Dasilva, and J. J. Lehtomäki, "Carrier aggregation/channel bonding in next generation cellular networks: Methods and challenges," *IEEE Netw.*, vol. 28, no. 6, pp. 34–40, Nov. 2014.
- [32] M. Deruyck, J. Wyckmans, W. Joseph, and L. Martens, "Designing UAV-aided emergency networks for large-scale disaster scenarios," *EURASIP J. Wireless Commun. Netw.*, vol. 2018, no. 1, p. 79, Dec. 2018.



GIANLUCA FONTANESI (Graduate Student Member, IEEE) received the B.Sc. and M.Sc. degrees in telecommunication engineering from Politecnico di Milan, Italy, in 2009 and 2012, respectively.

He has several years of industrial experience, focused on the development and testing of wireless systems, such as small cell base stations and air-to-ground communication. He commenced his Ph.D. study in the RF and the Microwave Group, University College Dublin (UCD), in October 2017, under the joint-supervision of Prof. A. Zhu and Dr. H. Ahmadi. His current research interests include future wireless networks, focusing on UAV aided wireless networks, and potential applications of machine learning techniques. He is a member of IRACON. He is also a member of the EIRSAT-1 Project, that aims to launch Ireland's first satellite and is led by students at University College Dublin as part of the ESA Fly Your Satellite! Programme. He is a Reviewer of several journals of the IEEE, including IEEE TRANSACTIONS ON VEHICULAR TECHNOLOGY and IEEE ACCESS.



ANDING ZHU (Senior Member, IEEE) received the Ph.D. degree in electronic engineering from University College Dublin (UCD), Dublin, Ireland, in 2004.

He is currently a Professor with the School of Electrical and Electronic Engineering, UCD. He has authored or coauthored more than 130 peer-reviewed journal and conference papers. His current research interests include high-frequency nonlinear system modeling and device characterization techniques, high-efficiency power amplifier design, wireless transmitter architectures, digital signal processing, and nonlinear system identification algorithms.

Prof. Zhu is an elected member of Administrative Committee (AdCom), the Chair of the Electronic Information Committee, and the Vice Chair of the Publications Committee. He is also the Chair of the MTT-S Microwave High-Power Techniques Committee. He has served as the Secretary of MTT-S AdCom in 2018. He was the General Chair of the 2018 IEEE MTT-S International Microwave Workshop Series on 5G Hardware and System Technologies (IMWS-5G) and the Guest Editor of the IEEE TRANSACTIONS ON MICROWAVE THEORY AND TECHNIQUES Special Issue on 5G Hardware and System Technologies. He is an Associate Editor of the *IEEE Microwave Magazine* and a Track Editor of the IEEE TRANSACTIONS ON MICROWAVE THEORY AND TECHNIQUES.



HAMED AHMADI (Senior Member, IEEE) received the Ph.D. degree from the National University of Singapore, in 2012. He was an Agency for Science Technology and Research (A-STAR) funded Ph.D. student at the Institute for Infocomm Research (I2R), National University of Singapore. Since then, he has been working with different academic and industrial positions in Ireland and U.K. He is currently an Assistant Professor with the Department of Electronic Engineering, University of York, U.K. He is also an Adjunct Assistant Professor with the school of Electrical and Electronic Engineering, University College Dublin, Ireland. He has published more than 50 peer-reviewed book chapters, journal, and conference papers. His current research interests include design, analysis, and optimization of wireless communications networks, airborne networks, wireless network virtualization, blockchain, the Internet-of-Things, cognitive radio networks, and the application of machine learning in small cell and self-organizing networks. He is a member of Editorial Board of IEEE ACCESS, *Frontiers in Blockchain*, and *Wireless Networks* (Springer). He is a Fellow of the U.K., Higher Education Academy and Networks working Group Co-Chair and a management committee member of COST Action 15104 (IRACON).

• • •